Impact of co- and counter-swirl on flow recirculation and liftoff of non-premixed oxy-flames above coaxial injectors

Arthur Degenève, Ronan Vicquelin, Clément Mirat, Jean Caudal, Thierry Schuller

Impact of co- and counter-swirl on flow recirculation and liftoff of non-premixed oxy-flames above coaxial injectors

A. Degeneve[a,b,*], R. Vicquelin[a], C. Mirat[a], J. Caudal[b], T. Schuller[a,c]

[a] *Laboratoire EM2C, CNRS, CentraleSupélec, Université Paris-Saclay, 3, rue Joliot Curie, 91192 Gif-sur-Yvette cedex, France*
[b] *Air Liquide, Centre de recherche Paris Saclay, Chemin de la Porte des Loges, B.P. 126, 78354 Les Loges en Josas, France*
[c] *Institut de Mécanique des Fluides de Toulouse, IMFT, Université de Toulouse, CNRS, Toulouse, France*

Abstract

Controlling the flame shape and its liftoff height is one of the main issues for oxy-flames to limit heat transfer to the solid components of the injector. An extensive experimental study is carried out to analyze the effects of co- and counter-swirl on the flow and flame patterns of non-premixed oxy-flames stabilized above a coaxial injector when both the inner fuel and the annular oxidizer streams are swirled. A swirl level greater than 0.6 in the annular oxidizer stream is shown to yield compact oxy-flames with a strong central recirculation zone that are attached to the rim of central fuel tube in absence of inner swirl. It is shown that counter-swirl in the fuel tube weakens this recirculation zone leading to more elongated flames, while co-swirl enhances it with more compact flames. These results obtained for high annular swirl levels contrast with previous observations made on gas turbine injectors operated at lower annular swirl levels in which central recirculation of the flow is mainly achieved with counter-rotating swirlers. Imparting a high inner swirl to the central fuel stream leads to lifted flames due to the partial blockage of the flow at the injector outlet by the central recirculation zone that causes high strain rates in the wake of the injector rim. This partial flow blockage is more influenced by the level of the inner swirl than its rotation direction. A global swirl number is then introduced to analyze the structure of the flow far from the burner outlet where swirl dissipation takes place when the jets mix. A model is derived for the global swirl number which well reproduces the evolution of the mass flow rate of recirculating gases measured in non-reacting conditions and the flame liftoff height when the inner and outer swirl levels and the momentum flux ratio between the two streams are varied.

Keywords:
Co-/counter-rotating, Swirl, Oxy-combustion, Liftoff, Flame stabilization

Colloquium: Stationary System / low Carbon

Length of the paper determined using Method 2.
Total length of the paper: less than 7.5 pages

The authors will pay color reproduction charges if applicable.

*Corresponding author:
Email address: arthur.degeneve@centralesupelec.fr (A. Degeneve)

Introduction

Conferring a rotational motion to the flow is widely used to extend the operational range of industrial injectors and increase flame compactness. A well-known advantage of a swirled flow is the formation of a central recirculation zone (CRZ) above a swirl threshold level. The CRZ favors flame stabilization downstream the injector thanks to low velocities and recirculation of hot burned gases [1].

In non-premixed systems, swirl is also known to improve mixing between a fuel jet injected in the center of a swirled annular oxidizer stream [2–7]. Swirl can also be conferred to the central fuel stream [8–10]. Adding inner swirl was shown to help lifting CH_4-air and H_2-air flames from the injector rim [8]. It was also used to control the liftoff height of C_3H_8-air flames [9]. In these studies, the outer-to-inner momentum flux ratio between the two streams is small $J \ll 1$. The way compact non-premixed swirled lifted flames could be stabilized above a coaxial injector was studied in [10] for a large range of momentum flux ratios $0.75 \leq J \leq 3$, inner and outer swirl levels and mass fractions of O_2 in the annular oxidizer stream $0.23 \leq Y_{O_2,2} \leq 0.5$. It was shown that the inner S_1 and outer S_2 swirl numbers are two independent parameters that can be tuned to adjust the flame liftoff height and flame shape. In these previous studies, swirl in the central and annular streams is conferred in co-rotating direction. The present study aims at covering counter-rotating configurations to reveal how the flow and flame structures are altered with respect to co-rotating operation.

Counter-swirl coaxial injectors are used in gas turbines operating in stratified premixed conditions [11–14] or in rocket engines with non-premixed flames [15, 16]. Counter-swirl increases the shear stress in the wake of the central injector rim [11–14] which favors mixing and atomization when the inner stream is liquid fuel or liquid O_2 [15].

For moderate swirl levels $S_2 < 0.6$ in the annular stream, it was established that counter-swirl in the central stream S_1 enhances gas recirculation in the CRZ for non-reacting jets [11–14]. Conversely, the CRZ disappears [12] or weakens [11, 14] when the same experiments are repeated without inner swirl $S_1 = 0$ or with an inner co-rotating swirler. Counter-swirl configurations therefore help the formation of a compact swirl-stabilized flame, when the inner S_1 and outer swirl S_2 levels are moderate [12]. Too large swirl levels lead to flashback or unacceptable pressure drop through the injector of gas turbines.

Many other industrial burners operate at a higher swirl level $S_2 \sim 1$ in the annular channel and feature a distinct behavior [17–19]. In these cases, a large CRZ prevails above the coaxial injector even in absence of inner swirl $S_1 = 0$. In co-rotating conditions, gas recirculation is enhanced and the CRZ is pushed further upstream because the inner swirl reduces the penetration of the central jet in the CRZ [18, 19]. The same trends are reported in reacting conditions [17]. A co-rotating inner swirler leads to a better mixing between the central fuel stream, the annular oxidizer swirled stream and the recirculating burned gases [18]. More recently, a counter-rotating swirler was shown to alter the shape of the CRZ of highly swirled flames stabilized above a coal burner [20].

This short literature review highlights how the flow produced by co- and counter-rotating swirlers leads to opposite effects on flow recirculation when a coaxial injector is operated at a moderate $S_2 < 0.6$ or at a high annular, say $S_2 > 0.8$, swirl number. These previous studies focus on a combustion region lying close to the injection plane $z/d_1 < 2$, where z denotes the axial coordinate along the combustor centerline axis and d_1 the diameter of the central fuel injector. Non-premixed flames are often anchored to the fuel nozzle rim $z/d_1 = 0$, but in many cases they may also stabilize further downstream $z/d_1 > 6$ [8–10]. Turbulent non-premixed methane/air swirling flames are almost never attached to the injector rim at ambient conditions [21], but O_2-enriched flames exhibit a wider variety of topologies [10]. These two features have motivated this study in which the impact of co- and counter-rotating swirl on the flame and flow patterns is characterized both at the outlet of the injector $z/d_1 = 0$ and further downstream up to $z/d_1 = 15$ with the help of optical diagnostics.

1. Experimental setup

Experiments are carried out on the Oxytec combustor, already used to investigate scaling relations for the length of non-premixed swirling oxy-flames [7] and the effects of inner co-swirl on flame stabilization [10].

The combustion chamber represented in Fig. 1(a) has a square cross section. The injector sketched in Fig. 1(b) comprises a central tube of inner diameter $d_1 = 6$ mm and thickness $e = 1$ mm that conveys the methane flow and an annular channel of outer diameter $d_2 = 20$ mm filled with O_2-enriched air.

Rotation is provided to both the central (1) and the annular (2) streams. Two swirl numbers S_i, $i = 1, 2$, are defined as $S_i = 2G_{i,\theta}/(d_i G_{i,z})$, where $G_{i,\theta}$ and $G_{i,z}$ are the tangential and axial momentum fluxes in the axial direction. These fluxes are determined by integration of

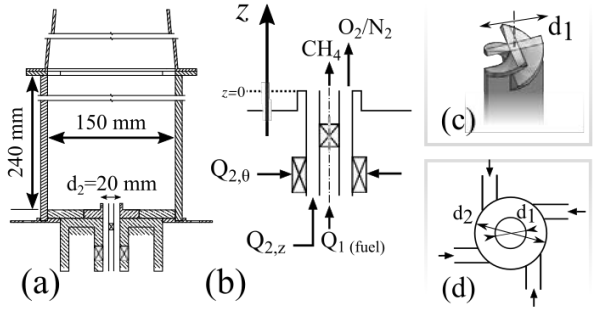

Figure 1: Sketch of the combustor. (a) Schematic of the Oxytec test rig. (b) Axial cut of the coaxial injector. (c) Isometric view of the axial inner swirler. (d) Transverse cut through the annular swirler.

the axial u_z and azimuthal u_θ velocities over the cross sections areas A_1 and A_2 of the central tube and of the annular channel: $G_{i,z} = \int_{A_i} \rho u_z^2 \mathrm{d}S$ is always positive, whereas $G_{i,\theta} = \int_{A_i} \rho r u_\theta u_z \mathrm{d}S$ is positive when $u_\theta > 0$ (counter-clockwise rotation), and negative when $u_\theta < 0$ (clockwise rotation).

The injection plane of the coaxial injector is located 5 mm above the back plane of the combustor to ease imaging the flame root and flame liftoff height. This injection plane defines the axial origin $z = 0$, and there is no recess between the central and the outer injection channel outlets. Four tangential slits generate a swirling motion, with swirl number S_2, in the annular oxidizer stream, as shown in Fig. 1(d). The distribution of the axial $Q_{2,z}$ and tangential $Q_{2,\theta}$ volume flow rates provides an adjustable swirl level S_2. Assuming a solid-body rotation of the flow and a uniform axial velocity, the geometrical swirl number S_2 in the annular channel is given by $S_2 = S_m/(1+Q_{2,z}/Q_{2,\theta})$, where $S_m = 1.23$ is deduced from geometrical considerations as in [7]. The inner stream is swirled with the help of seven removable sets of axial twisted vanes with trailing edge angles $\theta_1 = -60$, -50, -30, 0, 30, 50 and 60°, as illustrated in Fig. 1(c). The central fuel and annular oxidizer streams are counter-rotating when $\theta_1 < 0$ and co-rotating otherwise. With the same hypotheses on the velocity profiles as in the annular channel, the geometrical swirl number S_1 in the central tube is given by $S_1 = 1/2\tan(\theta_1)$.

The operating conditions covered in this study are reported in Table 1. The oxygen mass fraction is set to $Y_{O_2,2} = 0.40$ in the oxidizer stream as in [10]. This oxygen concentration leads to a broad range of liftoff transitions and changes of flame topology.

Except for dataset $\mathscr{D}_4$, the momentum flux ratio J between the annular (2) and central (1) streams is set to $J = \rho_2 u_{z,2}^2/\rho_1 u_{z,1}^2 = 0.75$, which is achieved by fixing the axial velocity in the inner fuel stream to $u_{z,1} = 23.3$ m.s^{-1} and the axial velocity in the annular oxidizer stream to $u_{z,2} = 15$ m.s^{-1}. This sets the thermal power $\mathscr{P}_{th} = 21.7$ kW, the global equivalence ratio $\phi = 0.91$ and the annular flow in the turbulent regime with a Reynolds number $Re_2 = \rho_2 u_{z,2} D_h/\mu_2 = 12,000$ based on the hydraulic diameter $D_h = 12$ mm. The swirl number in the central fuel stream is systematically varied from $S_1 = -0.87$ to 0.87. The swirl number in the annular channel is initially fixed to $S_2 = 0.85$.

These conditions are used to investigate the structure of the flow with Particle Image Velocimetry (PIV) with liquid (dataset $\mathscr{D}_1$) and solid particles (dataset $\mathscr{D}_2$). The spatial resolution of the PIV measurements is $\delta_x = 0.6$ and 1.2 mm for the non-reacting and reacting conditions, respectively. A sensitivity analysis, not shown here, has been carried out to verify that the velocity measurements and the position of the CRZ are left unchanged when slightly modifying the seeding of the flow and the duration time between the two laser impulses. For measurements in non-reacting conditions, the O_2-enriched mixture is replaced by air, but the inner stream is filled with methane to keep approximately the same gas density ratio as in reacting conditions. In reacting-conditions, PIV is synchronized with OH-PLIF measurements to track the unsteady position of the CRZ and the flame front ($\mathscr{D}_2$). The $Q_1(6)$ band of the hydroxyl radical is excited at $\lambda = 282.93$ nm with a laser delivering a 20 mJ energy pulse cadenced at 10 Hz. A full description of the optical diagnostics and image post-processing can be found in [22].

A broader set of flames (dataset $\mathscr{D}_3$ and $\mathscr{D}_4$) has been investigated with OH* chemiluminescence to determine the flame liftoff height z_f with respect to the nozzle rim when the inner swirl S_1, the outer swirl S_2 and the momentum flux ratio J are parametrically varied. The OH* intensity is collected at the wavelength $\lambda = 310$ nm, and the recording time $\Delta t = 30$ ms is long compared to the largest turbulent time scales of the flow. Images are averaged over 100 snapshots. The Otsu thresholding method [23] is chosen to infer the flame front location from images [7, 24]. The flame liftoff height z_f is determined as the lowest point of the Otsu contour. The standard deviation of the liftoff height $z_{f,rms}$ is limited

Table 1: Operating conditions. All experiments are conducted with a fixed O_2-fraction $Y_{O_2,2}$=0.4 and a Reynolds number Re_2 =12, 000.

Set	Diagnostic	Conditions	S_1	S_2	J
$\mathscr{D}_1$	PIV	non-reac.	±0.87	0.85	0.75
$\mathscr{D}_2$	PIV/PLIF	reac.	±0.87	0.85	0.75
$\mathscr{D}_3$	OH* chem.	reac.	±0.87	0.75	0.75
$\mathscr{D}_4$	OH* chem.	reac.	±0.87	0.6 – 1.1	0.75 – 3

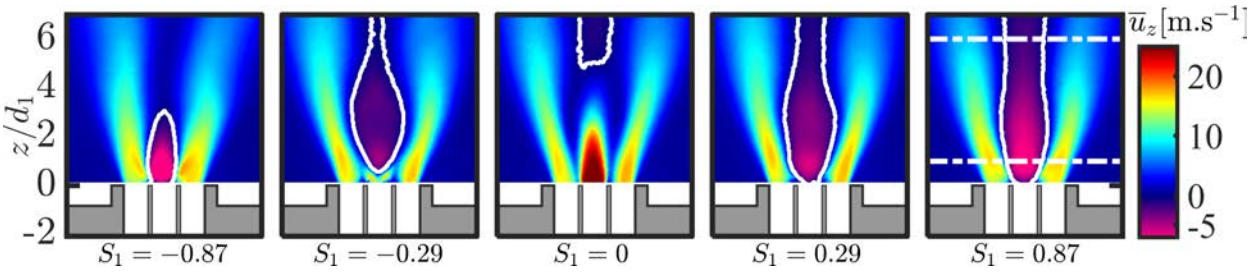

Figure 2: Mean axial velocity $\overline{u}_z$ for five coaxial jets in non-reacting conditions ($\mathscr{D}_1$ dataset) for $S_2 = 0.85$, $J = 0.75$. S_1 is varied from −0.87 to 0.87. The recirculation zone is delineated by the thick white contour.

to 10 % of its mean value z_f. A sensitivity analysis has been carried out to verify that the Otsu contour is left unaltered when the image brightness and contrast are varied. Finally, numerical simulations of one-dimensional flames have been performed to ensure that the temperature and OH* peaks both lie close to the reaction layer at $z = z_{st}$ (see suplemental material in [7]).

2. Impact of S_1 on the non-reacting flow

Impact of inner swirl on the structure of the non-reacting flow is investigated with PIV for five coaxial jets ($\mathscr{D}_1$ dataset) at a fixed annular swirl number $S_2 = 0.85$ and momentum flux ratio $J = 0.75$. The mean component of the axial velocity u_z is shown in an axial plane in Fig. 2. The azimuthal velocity profiles u_θ in a transverse plane are provided as supplemental material. The magnitude of S_1 and the swirl direction have a considerable impact on the CRZ position delineated in white in Fig. 2. The location of the CRZ depends on the absolute value $|S_1|$ of the inner swirl number. In the absence of inner swirl $S_1 = 0$, the central fuel stream pushes the CRZ away from the injector. When $|S_1|$ increases, the CRZ moves upstream and establishes closer to the injector outlet. Let Q_r be the recirculating volume flow rate in the CRZ at some fixed distance above the injector, $Q_r = -\pi \int_{-r^*}^{r^*} \overline{u}_z r \mathrm{d}r$, where r^* denotes the radial coordinate where the axial velocity is zero: $\overline{u}_z(-r^*) = \overline{u}_z(r^*) = 0$. This flowrate is determined at the heights $z/d_1 = 1$ and 6, represented as white dashed horizontal lines in Fig. 2. Results are shown in Table 2.

Table 2: Recirculating volume flow rate Q_r divided by the injected volume flow rate $Q_0 = 16.6$ m^3.h^{-1}, ratio of tangential momentum flux and global swirl number S_{1+2} as a function of inner swirl S_1 for different heights z/d_1 above the injector. $S_2 = 0.85$. $J = 0.75$.

S_1	z/d_1	−0.87	−0.29	0	0.29	0.87
Q_r/Q_0(%)	1	4.4	1.4	0	5.0	5.8
Q_r/Q_0(%)	6	0	0.02	0.37	0.39	1.3
$G_{\theta,1+2}/G_{\theta,1+2}^{S_1=0}$	4	0.86	0.99	1.0	1.07	1.05
S_{1+2} (Eq. 1)		0.71	0.73	0.74	0.75	0.78

Results are first analyzed close to the injector outlet, at height $z/d_1 = 1$. The recirculating flowrate Q_r increases with the swirl number S_1 for both co- and counter-rotating directions, indicating that the inner swirl locally favors stabilization of the CRZ at the outlet of the injector. This feature highlighted here for a fixed annular swirl number $S_2 = 0.85$ contrasts with the dynamics observed above a gas turbine injector operated at a lower swirl level $S_2 \simeq 0.5$ [11–14]. In this latter case, the CRZ is enhanced only with counter-swirl flow and disappears in co-rotating direction. The origin of this difference is discussed at the end of the section.

Figure 2 also shows that the impact of S_1 on the flowfield is totally different further downstream away from the injector outlet. In the far-field, the presence of a CRZ and the magnitude of the recirculating flowrate Q_r also depend on the rotation direction of the two swirling jets. At $z/d_1 = 6$, Q_r is maximum for co-swirl when $S_1 = 0.87$ and decreases with S_1 until the CRZ vanishes for a counter-swirl at $S_1 = -0.87$.

The far-field structure of the swirling flow may be interpreted with the help of a global swirl number $S_{1+2} = 2G_{1+2,\theta}/(d_2 G_{1+2,z})$ when the inner and outer jets have mixed. Noting that $G_{1+2,k} = G_{1,k} + G_{2,k}$ for $k = z, \theta$ and that the axial momentum fluxes are linked by $G_{2,z}/G_{1,z} = J(A_2/A_1)$, the global swirl number S_{1+2} therefore only depends on S_1, S_2 and J and may be written as:

$$S_{1+2} = \frac{d_1}{d_2}\alpha S_1 + (1-\alpha)S_2 \qquad (1)$$

where $\alpha = (1 + JA_2/A_1)^{-1}$ lies between 0 and 1. The tangential momentum flux $G_{1+2,\theta}$ measured at the height $z/d_1 = 4$ is reported in Table 2. It is found that $G_{1+2,\theta}$ is minimum for counter-rotating swirls at $S_1 = -0.87$ and maximum for co-rotating direction when $S_1 = 0.29$ or 0.87. In agreement with previous studies [11, 12, 20], the swirling motion decreases more rapidly for counter-

swirl jets. This evolution leads to the disappearance of the CRZ at $z/d_1 = 6$ for $S_1 = -0.87$ after the jets have mixed in Fig. 2.

The global swirl number S_{1+2} predicted by Eq. (1) is also reported in Table 2. As discussed later, S_{1+2} only slightly changes when S_1 is varied because S_{1+2} is less sensitive to variations of S_1 than to modifications of S_2. The evolution of the recirculating flowrate Q_r measured at height $z/d_1 = 6$ shows a good correlation with the global swirl number S_{1+2}. This feature confirms that the presence of a CRZ far from the injector outlet results from the global swirl motion after the inner and the outer jets have mixed. When the jets are counter-rotating with $S_1 = -0.87$, the global swirl number $S_{1+2} = 0.71$ is minimum, leading to the disappearance of the CRZ observed at $z/d_1 = 6$ in Fig. 2. Conversely, when co-rotating, the tangential momentum $G_{1,\theta}$ and $G_{2,\theta}$ accumulate while mixing, which yields the highest recirculation flow rate Q_r for $S_1 = 0.87$ at $z/d_1 = 6$.

The main observations are synthesized. In the present study $S_2 = 0.85$ is high, swirling the inner stream leads to two distinct near-field and far-field behaviors. (i) At the injector outlet, inner swirl promotes the formation of a CRZ depending on the absolute value of S_1. Change of the jet rotation direction barely alters the CRZ in the near-field region. (ii) Further downstream, the inner jet also affects stabilization of the CRZ. In this region, the rotation direction has a major influence on the CRZ, which is well captured by considering the global swirl level S_{1+2} defined by Eq. (1).

The mechanisms leading to the formation of the CRZ above a coaxial injector are now further scrutinized by reporting the results from Fig. 2 together with results from past studies in a diagram shown in Fig. 3. Rise of the adverse pressure gradient $\partial p/\partial z$ on the centerline axis in a swirling flow originates from the decay of the azimuthal velocity given by [3, 11, 12]:

$$\left.\frac{\partial p}{\partial z}\right|_{r=0} \simeq -2\int_0^R \rho \frac{|u_\theta|}{r}\frac{\partial |u_\theta|}{\partial z}\mathrm{d}r \qquad (2)$$

where $r = R$ is the radial position at the sidewalls.

A first configuration leading to the formation of a CRZ in Fig. 2 is associated to a high value of the inner swirl number $|S_1| > 0.6$. This region is noted I in Fig. 3. Decay of u_θ in the central stream is sufficient to increase the adverse pressure gradient in Eq. (2) leading to a CRZ located at the outlet of the central tube. This mechanism prevails in [20] or in Fig. 2 with $S_1 = \pm 0.87$. Another combination is when $|S_1| < 0.6$. If S_2 is high enough, the tangential momentum remaining after mixing of the central and the annular jets can generate a CRZ. This second mechanism takes over further downstream the injector outlet and is well predicted by the global swirl number S_{1+2} defined by Eq. (1). A rough limit is defined by $S_{1+2} \gtrsim 0.7$ that is added in Fig. 3 and delineates region II. This situation is observed when $S_1 = 0$ in [3, 5], for $S_1 \geq 0$ in [17–19] or in Fig. 2 for $S_1 \geq 0$. The last situation corresponds to coaxial jets with moderate swirl levels S_1 and $S_2 \sim 0.5$ that produce a CRZ only when they are counter-rotating. In this configuration, noted III in Fig. 3, the decay of the azimuthal velocity $\partial|u_\theta|/\partial z$ is faster for counter-swirling jets, leading to the formation of a CRZ [11, 12].

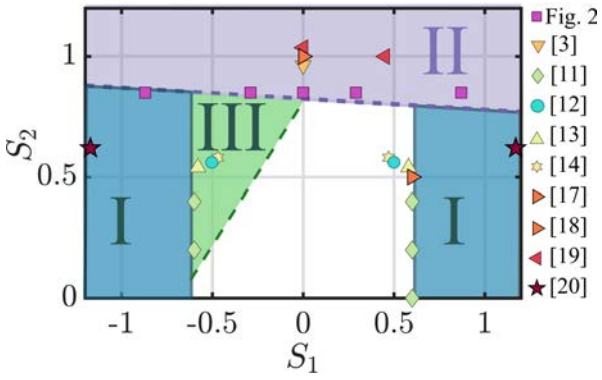

Figure 3: Map of the different regimes with a CRZ above the coaxial injector as a function of S_1 and S_2. I) Region with $|S_1| > 0.6$. II) Region with global swirl number $S_{1+2} > 0.7$. III) Counter-swirl region with $S_2 < 0.6$

The three regimes identified in Fig. 3 enable to report the results from many past studies in which a CRZ has been obtained for different swirl levels in the inner or outer streams, and with different swirler geometries. This diagram highlights that coaxial jets with moderate swirl levels feature an intense CRZ when counter-rotating [11–14] and a weak [12] or no CRZ [11, 14] when co-rotating. The experiments conducted in this study with a high swirl level in the annular jet indicate that swirling the inner jet in counter- and co-rotating direction leads to the formation of a CRZ and that its position directly depends on the values of $|S_1|$ and S_{1+2}.

3. Impact on S_1 on the flame structure and flow field

The structure of the reacting flow is analyzed with the PIV/OH-PLIF setup for the same injection conditions as in Fig. 2 (dataset $\mathscr{D}_2$). Mean OH-PLIF images are represented in Fig. 4 superimposed to the velocity field in the axial plane of the burner. Instantaneous snapshots of the synchronized PIV and OH-PLIF diagnostics are provided in the supplemental material for the same operating conditions.

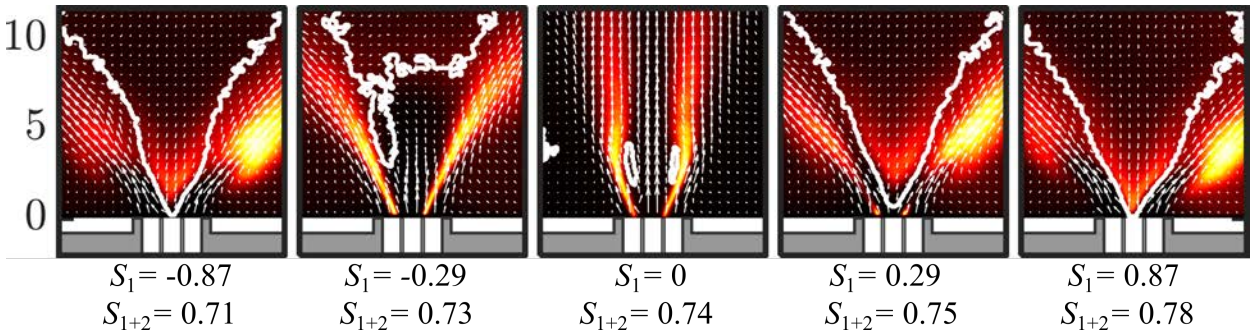

Figure 4: OH-PLIF/PIV measurements for flames at $S_2 = 0.85$, $J = 0.75$ and S_1 ($\mathscr{D}_2$ dataset) varying from $S_1 = -0.87$ to 0.87. Mean OH-PLIF signal is shown in color scale. The average velocity field is superimposed with white arrows. The recirculation zone is delineated by the thick white contours.

Figure 4 shows that combustion has disrupted the flow field. In the absence of inner swirl $S_1 = 0$, the CRZ is pushed downstream compared to non-reacting operation in Fig. 2. The flame lies in this case in the jet-like regime in agreement with results from Chen *et al.* [5]. When the inner swirl level slightly increases to $|S_1| = 0.29$, the flame features a CRZ for both co- and counter-rotating directions. In these cases, the width and length of the CRZ are drastically enhanced compared to non-reacting conditions in Fig. 2. Enhancement of gas recirculation is also in agreement with previous studies reporting that the heat release pushes the CRZ of swirl-stabilized flames more upstream [3, 12]. The inner swirl level therefore has a considerable impact on the flame topology. A slight increase of $|S_1|$ in Fig. 4 leads to the transition of the flame from a jet-like regime for $S_1 = 0$ to a CRZ regime when $|S_1| = 0.29$ but the flame remains anchored on the central tube. It can be noticed that flame with $S_1 = -0.29$ is not perfectly symmetric. This is attributed to a small tilting of the inner tube with respect to the axis of the outer channel. This asymmetry remains however small. When the inner swirl is further increased to $|S_1| = 0.87$, the CRZ is pushed closer to the injector outlet, and the reaction layer becomes detached from the central injector rim.

The position of the CRZ in Fig. 4 is used to explain the flame liftoff transition as sketched in Fig. 5. When $|S_1| \leq 0.29$, the flame is anchored on the central fuel rim. A reaction layer starts in the wake of the injector rim at the interface between the central fuel stream and the annular oxidizer stream. When $|S_1| = 0.87$, the CRZ protrudes inside the central injector leading to a partial flow blockage of the inner fuel stream. The central jet is thus diverted in the radial direction with high velocities. This drastically increases the shear stress in the wake of the fuel injector rim. Enhancement of strain leads to extinction of the diffusion reaction layer in the wake of injector rim and the flames stabilizes further downstream close to the CRZ.

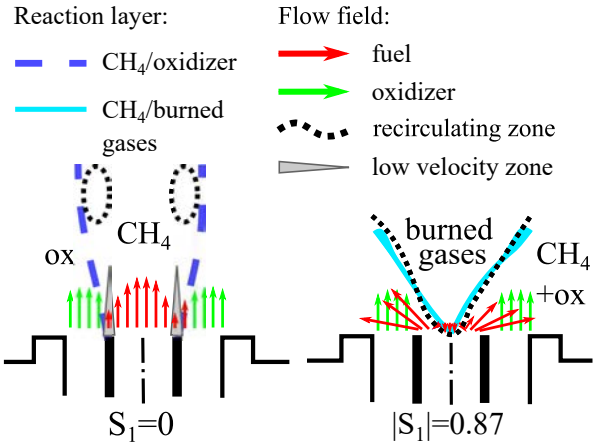

Figure 5: Schematic representation of the two causes leading to flame liftoff when $|S_1| = 0.87$.

When the inner swirl number is high enough $|S_1| \geq 0.6$ to sustain a CRZ by itself, partial flow blockage of the central fuel stream locally occurs for both co- and counter-rotating directions. The flame liftoff height is in this case the same for $S_1 = \pm 0.87$ as shown by Fig. 4. When the inner swirl drops below $|S_1| < 0.6$, the presence of the CRZ at the injector outlet also depends on the interaction between the two swirling jets. In that case, the CRZ in Fig. 4 is located more upstream for $S_1 = 0.29$ than for $S_1 = -0.29$.

Impact of the co- and counter-rotating direction of the inner swirl has been investigated for a broader range of operating conditions ($\mathscr{D}_4$ dataset) by varying S_1 between -0.87 and 0.87, S_2 from 0 to 1.1 and J from 0.75 to 3, leading to about 340 operating conditions. This parametric analysis confirms that the rotation di-

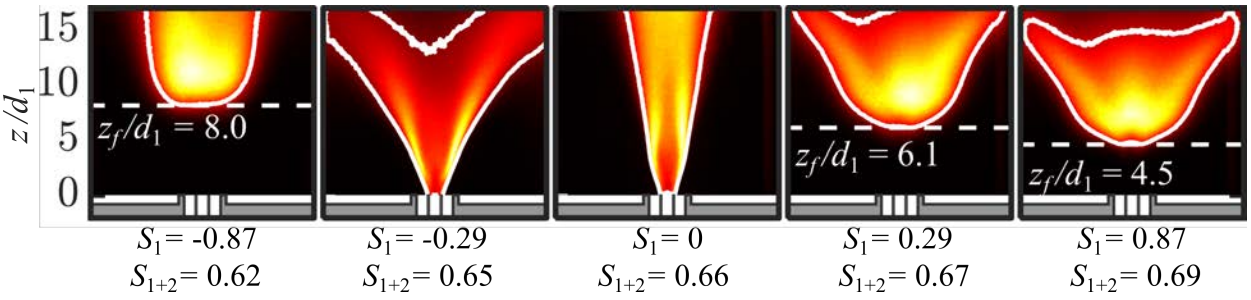

Figure 6: OH* Chemiluminescence intensity signal for oxy-flames featuring different inner swirl numbers from $S_1 = -0.87$ to $S_1 = 0.87$ ($\mathscr{D}_3$ dataset, $S_2 = 0.75$ and $J = 0.75$). The Otsu contour [23] corresponds to the thickened white contour. The global swirl number S_{1+2} defined by Eq. (1) is reported at the bottom of each flame.

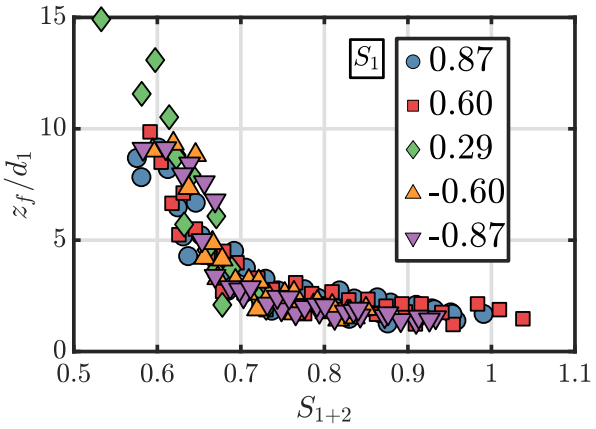

Figure 7: Dimensionless liftoff height z_f/d_1 with respect to the global swirl number S_{1+2} as defined by Eq. (1). Only flames with a liftoff height higher than $z_f/d_1 > 0.4$ have been retained. Data points are colored by the value of the inner swirl number ($\mathscr{D}_4$ dataset).

rection barely alters the flame liftoff transition when the inner swirl number is high enough $|S_1| > 0.6$. For low swirl numbers $|S_1| < 0.6$, an example where the rotation direction changes the liftoff transition is displayed in Fig. 6 with OH* chemiluminescence images ($\mathscr{D}_3$ dataset). In this case, the flame is lifted above the injector for $S_1 = 0.29$ and anchored to the nozzle rim for $S_1 = -0.29$.

4. Impact of S_1 for lifted flames

Impact of inner swirl S_1 in co- and counter-rotating directions is now investigated only for the lifted flames stabilized downstream the coaxial injector. Three of them are represented in Fig. 6 showing that the flame leading edge position z_f is very sensitive to the rotation direction, and therefore to the amount of swirl remaining after the jets have mixed. The value of the global swirl number S_{1+2} indicated in Fig. 6 shows a very good correlation with the evolution of the liftoff height z_f. When S_1 is counter-rotating, S_{1+2} decreases and the flame is pushed downstream, whereas S_{1+2} increases and z_f decreases when S_1 is co-rotating.

The analysis proceeds by plotting the flame liftoff height z_f/d_1 with respect to S_{1+2} in Fig. 7 for all the lifted flames investigated when $z_f/d_1 > 0.4$. This corresponds to a series of 190 flames obtained for different values of S_1, S_2 and J. The flames operated at $S_1 = 0$ or -0.29 could not be lifted and are therefore discarded [10]. Data colored by the value of the inner swirl number S_1 collapse on a single curve in Fig. 7 for both co- and counter-rotating configurations. The liftoff height z_f/d_1 decreases when S_{1+2} increases.

Analysis of Eq. (1) for S_{1+2} is used to get further insight on the structure of flow exhausting from a dual swirl coaxial injector. A first order perturbation analysis yields $\delta S_{1+2} = (d_1/d_2)\alpha\delta S_1 + (1-\alpha)\delta S_2 + \beta\alpha^2 A_2/A_1 \delta J$, with $\beta = (S_2 - d_2/d_1 S_1)$. The ratio A_2/A_1 is often large for coaxial injectors (9.3 in the present study) leading to small values for α when J is not too small. In this case, changing the outer swirl number S_2 has a much bigger impact on S_{1+2} than changing S_1. This explains why variations of the inner swirl number from $S_1 = -0.87$ to 0.87 in Fig. 6 only reduce z_f/d_1 from 8.0 to 4.5. In configurations with a small annular velocity, α is equal to unity: the coaxial jet is governed by the inner swirl number S_1, as in [8, 9].

For all the investigated lifted flames, the parameter β is positive $\beta > 0$. Increasing the momentum flux ratio J therefore reduces S_{1+2}, leading to a reduction of the flame liftoff height z_f/d_1. By noticing that $S_2 - S_{1+2} = \alpha\beta$, the relationship between the inner and the outer swirl numbers $\beta > 0$ also shows that the global swirl number is smaller than the one in the annular channel $S_{1+2} < S_2$. This number S_{1+2} must however not be used to interpret detachment of the flame front from the central injector rim. In Fig. 6, the flame is lifted for $S_{1+2} = 0.62$, 0.67 and 0.69 but anchored for $S_{1+2} = 0.65$

and 0.66. Liftoff of O_2-enriched flames is controlled by the value of S_1 leading to a partial blockage of the fuel stream at the outlet of the central injector as described in the previous section.

The global swirl number S_{1+2} therefore constitutes a useful dimensionless number to determine the evolution of the flame liftoff height z_f/d_1 of oxy-flames exhausting from a dual swirl injector. It models the influence of S_1, S_2 and J relying on the hypothesis that the inner and outer jet momentums have mixed.

Conclusion

Impact of co- and counter-rotating directions of swirl in a coaxial injector has been investigated for O_2-enriched air methane diffusion flames with a parametric approach and the help of optical diagnostics in reacting and non-reacting conditions. It has been found that the dynamics of a counter-rotating swirl injector with a high annular swirl number exhibits a different behavior than the flow obtained from injectors with a moderate annular swirl number. In this work, counter-swirl in the inner fuel stream weakens the central recirculation zone while co-swirl enhances it. One major outcome of this study regarding co- and counter-swirls is to separate near-field effects occurring at the outlet of the injector from swirl dissipation happening further downstream after the jets have mixed.

At the outlet of the injector, transition to liftoff for O_2-enriched flames is caused by the partial blockage of the inner fuel stream when the central recirculation zone stabilizes at the outlet of the fuel injector. This flow blockage leads to high transverse velocities and high strain rates in the wake of the injector rim and is more influenced by the magnitude of the inner swirl number $|S_1|$ than its rotation direction.

Further downstream, after the inner and outer jets have mixed, the liftoff height z_f/d_1 of the non-premixed oxy-flames exhausting from a dual swirl injector has been shown to scale with a global swirl number S_{1+2} defined by Eq. (1) for a large range of operating conditions $-0.87 \leq S_1 \leq 0.87$, $0.6 \leq S_2 \leq 1.1$, $0.75 \leq J \leq 3$, for both co- and counter-swirl configurations.

References

[1] N. Syred, N. Chigier, J. Beer, Flame stabilization in recirculation zones of jets with swirl, Proc. Comb. Inst. 13 (1) (1971) 617–624.

[2] N. A. Chigier, J. M. Beér, Velocity and static-pressure distributions in swirling air jets issuing from annular and divergent nozzles, J. Basic Eng. 86 (4) (1964) 788–796.

[3] V. Tangirala, R. Chen, J. F. Driscoll, Effect of heat release and swirl on the recirculation within swirl-stabilized flames, Combust. Sci. Technol 51 (1-3) (1987) 75–95.

[4] R.-H. Chen, J. F. Driscoll, The role of the recirculation vortex in improving fuel-air mixing within swirling flames, Proc. Comb. Inst. 22 (1) (1989) 531–540.

[5] R.-H. Chen, J. F. Driscoll, J. Kelly, M. Namazian, R. Schefer, A comparison of bluff-body and swirl-stabilized flames, Combust. Sci. Technol. 71 (4-6) (1990) 197–217.

[6] D. Feikema, R.-H. Chen, J. F. Driscoll, Enhancement of flame blowout limits by the use of swirl, Combust. Flame 80 (2) (1990) 183–195.

[7] A. Degenève, R. Vicquelin, C. Mirat, B. Labegorre, P. Jourdaine, J. Caudal, T. Schuller, Scaling relations for the length of coaxial oxy-flames with and without swirl, Proc. Comb. Inst. 37 (4) (2019) 4563–4570.

[8] S. Yuasa, Effects of swirl on the stability of jet diffusion flames, Combust. Flame 66 (2) (1986) 181–192.

[9] M. Cha, D. Lee, S. Chung, Effect of swirl on lifted flame characteristics in nonpremixed jets, Combust. Flame 117 (3) (1999) 636–645.

[10] A. Degeneve, C. Mirat, J. Caudal, R. Vicquelin, T. Schuller, Effects of swirl on the stabilization of non-premixed oxygen enriched flames above coaxial injectors, J. Eng. Gas Turb. Power, accepted.

[11] B. T. Vu, F. Gouldin, Flow measurements in a model swirl combustor, AIAA Journal 20 (5) (1982) 642–651.

[12] F. Gouldin, J. Depsky, S.-L. Lee, Velocity field characteristics of a swirling flow combustor, AIAA journal 23 (1) (1985) 95–102.

[13] J. Ramos, H. Somer, Swirling flow in a research combustor, AIAA journal 23 (2) (1985) 241–248.

[14] J. Mehta, H.-W. Shin, D. Wisler, Mean velocity and turbulent flow-field characteristics inside an advanced combustor swirl cup, in: 27th Aerospace Sciences Meeting, 1989, p. 215.

[15] Y. Hardalupas, J. Whitelaw, Characteristics of sprays produced by coaxial airblast atomizers, J. Propul. Power 10 (4) (1994) 453–460.

[16] M. Soltani, K. Ghorbanian, M. Ashjaee, M. Morad, Spray characteristics of a liquid–liquid coaxial swirl atomizer at different mass flow rates, Aerosp. Sci. Technol. 9 (7) (2005) 592–604.

[17] J. Truelove, T. Wall, T. Dixon, I. M. Stewart, Flow, mixing and combustion within the quarl of a swirled, pulverised-coal burner, Proc. Comb. Inst. 19 (1) (1982) 1181–1187.

[18] T. Dixon, J. Truelove, T. Wall, Aerodynamic studies on swirled coaxial jets from nozzles with divergent quarls, J. Fluids Eng. 105 (2) (1983) 197–203.

[19] T. Mahmud, J. Truelove, T. Wall, Flow characteristics of swirling coaxial jets from divergent nozzles, Journal of fluids engineering 109 (3) (1987) 275–282.

[20] Y. Sung, G. Choi, Non-intrusive optical diagnostics of co-and counter-swirling flames in a dual swirl pulverized coal combustion burner, Fuel 174 (2016) 76–88.

[21] H. K. Kim, Y. Kim, S. M. Lee, K. Y. Ahn, Emission characteristics of the 0.03 mw oxy- fuel combustor, Energy Fuels 20 (5) (2006) 2125–2130.

[22] A. Degenève, P. Jourdaine, C. Mirat, J. Caudal, R. Vicquelin, T. Schuller, Effects of a diverging cup on swirl number, flow pattern and topology of premixed flames, J. Eng. Gas Turb. Power 141 (3) (2019) 031022.

[23] N. Otsu, A threshold selection method from gray-level histograms, IEEE Trans. Syst. Man Cybern 9 (1) (1979) 62–66.

[24] Q. Wang, L. Hu, X. Zhang, X. Zhang, S. Lu, H. Ding, Turbulent jet diffusion flame length evolution with cross flows in a subpressure atmosphere, Energy Convers. Manag. 106 (2015) 703–708.